ELSEVIER

Physica C 288 (1997) 178–184

PHYSICA C

# Preparation of double-sided $YBa_2Cu_3O_{7-\delta}$ film by hot-wall type MOCVD

Yoshiaki Ito [a,*], Yutaka Yoshida [a,b], Morihiro Iwata [b], Yoshiaki Takai [b], Izumi Hirabayashi [a]

[a] *Superconductivity Research Laboratory, International Superconductivity Technology Center, Nagoya 456, Japan*
[b] *Department of Electrical Engineering, Nagoya University, Nagoya 464-01, Japan*

Received 4 June 1997; accepted 30 June 1997

**Abstract**

A hot-wall type metal organic chemical vapor deposition (MOCVD) apparatus has been developed for the deposition of the $YBa_2Cu_3O_{7-\delta}$ (YBCO) films on arbitrary shaped substrates using liquid metal organic sources. By improving the reactor shape and gas flow of the source materials, we succeeded in fabricating the double-sided YBCO films and the YBCO-coated conductor on oxide fiber. The YBCO films on both sides of the $LaAlO_3$ (100) substrate showed almost the same superconducting properties. The films deposited on the facet of the single crystalline $SrTiO_3$ fiber showed the biaxial alignment in the *ab*-plane, that is suitable as a seed crystalline layer for successive liquid phase epitaxial (LPE) growth.


*Keywords:* $YBa_2Cu_3O_{7-\delta}$; MOCVD; Liquid sources; Fiber; Double-sided

## 1. Introduction

One of the most promising applications of high-$T_c$ superconducting materials are microwave devices. For the high $Q$ circuit, thin films with low microwave surface resistance are required. A double-sided coated superconducting film is the best for this purpose. The circuits made of the double-sided $YBa_2Cu_3O_{7-\delta}$ (YBCO) films have much lower insertion loss, compared with the circuits with a normal metal (Au) ground plane [1]. For the preparation of the double-sided films, a lot of studies have been done using various vapor deposition techniques, such as the thermal co-evaporation method [2], off-axis magnetron sputtering [3] and metalorganic chemical vapor deposition (MOCVD) [4]. In order to grow the film on the second side by these methods, it is necessary to turn over the substrate, and deterioration of quality occurs on the first side of the film due to heating. On the other hand, in order to increase $J_c$ or $I_c$ of YBCO coated conductor for power cable applications, biaxially in-plane alignment is required and IBAD [5] or RABiTS [6] methods realized it as the aligned oxide buffer layer on metallic substrates. Recently we have proposed liquid phase epitaxy (LPE) grown YBCO wires and prepared fine single crystalline oxide fibers as substrates for this purpose

* Corresponding author. Tel.: +81 52 8714002; fax: +81 52 8714090; e-mail: hori-ito@istec.or.jp

0921-4534/97/$17.00 
*PII* S0921-4534(97)01573-6

[7]. We have two different aims for CVD growth on oxide fibers. One is the seed crystal layer formation for LPE growth. The seed layer of YBCO thin film makes the LPE pseudo homo-epitaxial one and realizes stable growth.

In this work, we present the deposition of the YBCO films (1) on double-sided substrates, and (2) on fine oxide fibers by hot-wall type MOCVD using liquid sources. We show the details of apparatus and report on homogeneity of the double-sided YBCO films on the $LaAlO_3$ substrate. We also mention the results of the deposition on the fine single crystalline $SrTiO_3$ fiber and successive LPE deposition for YBCO coated conductors.

## 2. Experimental

### 2.1. Reactor structure

Fig. 1 shows the schematic drawing of the hot-wall type MOCVD apparatus. The source gas supplying system is essentially the same as our conventional cold-wall MOCVD apparatus [8]. However, the reactor shape and the heating system are completely different. The heating method is indirect, that is, radiation from an infrared lamp (Infrared Image Furnace) heats a SiC tube around the quartz reactor tube and then the heated SiC tube heats the atmosphere in the quartz reactor tube. This quartz reactor tube is a double tube and the source gas is introduced from the outside tube to the inside one and decomposed around the deposition area. The substrate (or fiber) was fixed at the end of $Al_2O_3$ pipe. All of the organic compounds were used in liquid state to improve reproducibility of the composition in the deposited film [9,10]. So the decomposition of the source materials is caused by heat from the SiC tube before they reach the precise sample position and also solidification occurs at the part of which temperature is lower than their melting points. We have to keep transport line temperatures between their melting points and decomposition temperatures of source materials. The source gas flow is also important for stable deposition. Sometimes the source gas flows upstream due to the large temperature gradient between the upper and the lower parts of the reactor.

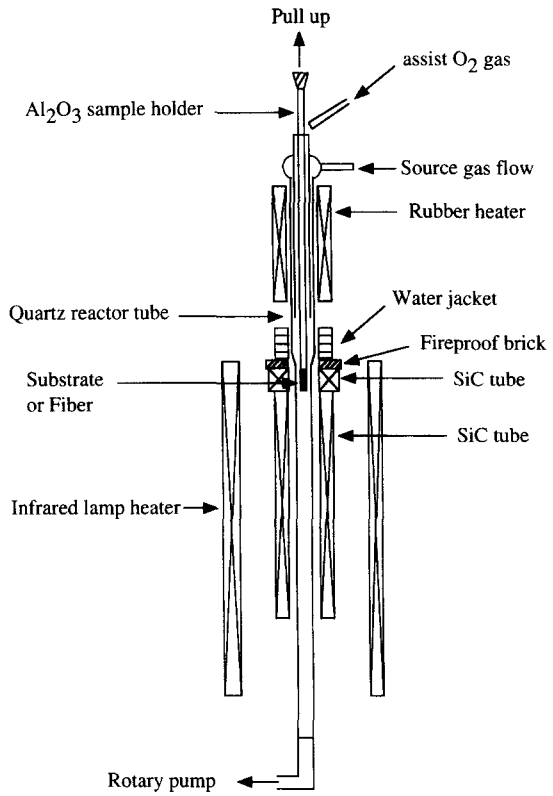


Fig. 1. Schematic drawing of the reactor.

In order to resolve these problems, we made some improvements of the reactor as follows: (1) prevention of source decomposition except at the precise deposition area, (2) improvement of the source gas flow, and (3) prevention of the source solidification in the quartz reactor tube. We changed the deposited position to the top of the SiC tube and a cooling water pipe and a fireproof brick to prevent the unwanted decomposition of the source materials. The necessary $O_2$ gas was introduced from the top of the quartz reactor tube and the exhaust gas was removed by a rotary pump in order to make source gases reach the substrate. Furthermore, a rubber heater was set up above the cooling water pipe to prevent the solidification of the source materials. After making the above-mentioned improvements, we succeeded in fabricating YBCO films on the substrate, although a large temperature gradient still remains around the deposition area. Fig. 2 shows atmospheric tempera-

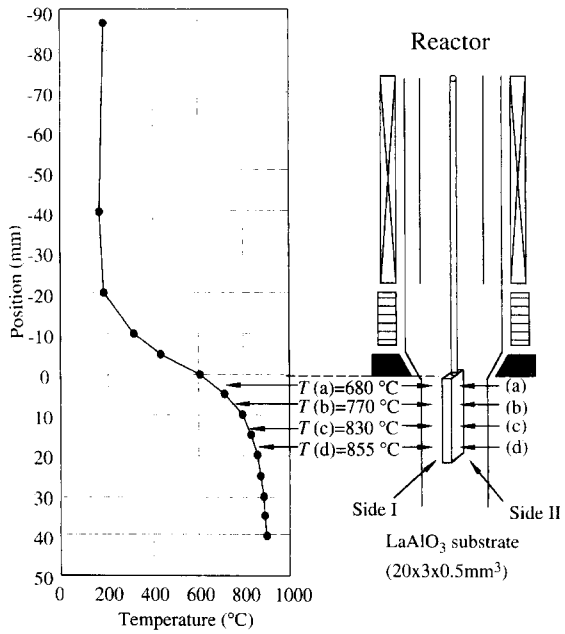


Fig. 2. Distribution of atmospheric temperature in the reactor. $T$(a)–$T$(d) correspond to atmospheric temperatures around the points (a)–(d), respectively.

ture around the sample in the reactor. The substrate (or fiber) is placed just below the fireproof brick. The atmospheric temperatures at the top and the bottom of the substrate ($T$(a) and $T$(d)) were 680°C and 855°C, respectively.

### 2.2. Deposition conditions

The typical conditions for our depositions are shown in Tables 1 and 2. The source materials used are yttrium-tris-(2,2,6,6-tetramethylheptane-3,5-dionate) 4-*t*-butylpyridine-*N*-oxide adduct ($Y(DPM)_3 \cdot 4tBuPyNO$), barium-bis-(2,2,6,6-tetramethylheptane-3,5-dionate) 2-tetraethylenepentamine adduct ($Ba(DPM)_2 \cdot 2tetraene$) and copper-bis-(2,2,6-trimethylheptane-3,5-dionate) ($Cu(TMHPD)_2$). All source materials were heated above their melting points and used in liquid state. The substrate was the double-side-polished $LaAlO_3$ ($20-30 \times 3 \times 0.5$ $mm^3$) or the fine $SrTiO_3$ single crystalline fibers ($0.4^{\phi} \times \ell$ 20–62 mm), that was fixed at the bottom of $Al_2O_3$ pipe sample holder. Deposition temperature varied from 680 to 855°C as shown Fig. 2, which was the temperature of atmosphere around the deposition area.

Table 1
Source material, mass flow and source temperature

| Source materials | Mass flow (Ar gas) | Source temperature |
|---|---|---|
| $Y(DPM)_3 \cdot 4tBuPyNO$ | 11–51 sccm | 135°C |
| $Ba(DPM)_2 \cdot 2tetraene$ | 29–75 sccm | 150°C |
| $Cu(TMHPD)_2$ | 1–3 sccm | 121–123°C |

Table 2
Substrate and conditions for deposition

| | |
|---|---|
| Substrate | Double-side-polished $LaAlO_3$ (100), $SrTiO_3$ (100) ($20-30 \times 3 \times 0.5$ $mm^3$), $SrTiO_3$ fiber ($0.4^{\phi} \times \ell$ 20–62 mm) |
| $O_2$ flow | 500–700 sccm |
| Total pressure | 6 Torr |
| $O_2$ partial pressure | 3–5 Torr |
| Deposition temperature | 680–855°C |
| Deposition time | 0.5–2 h |
| Growth rate | 0.1–0.5 μm/h |
| Pulling speed | 0–90 mm/h |

### 2.3. Characterizations

The grown films were characterized by X-ray diffraction (XRD) measurement. In-plane alignment of the films was determined by X-ray pole figure measurement. The surface morphology of the films was observed by scanning electron microscope (SEM) and atomic force microscope (AFM). Atomic composition of YBCO was determined by inductive coupled plasma spectrometry (ICP). The critical temperature ($T_c$) of the grown films was measured by four probe resistance measurement. The DC magnetic susceptibility of the films was measured by a SQUID magnetometer in the field of 10 G.

## 3. Results

### 3.1. Identical properties of each side of the double-sided film

Fig. 3 shows the $\theta$–$2\theta$ scan and the pole figure of (102) reflection of the YBCO film grown on both

sides of the double-side-polished $LaAlO_3$ (100) substrate. (00$n$) peaks ($n$ = 1–7) of YBCO are present in Fig. 3, which indicates that both sides of the film are highly $c$-axis oriented. The pole figure of (102) reflection of the YBCO films on the $LaAlO_3$ (100) substrate indicates a four-fold symmetry at $\alpha = 33°$. Here, we set $\beta = 0°$ parallel to $< 100 >$ of the $LaAlO_3$ substrate. The in-plane alignment of $ab$-axis of the film and the crystallographic relation between YBCO and $LaAlO_3$ is obtained as $< 100 >$ or $< 010 >$ of YBCO$\| < 100 >$ of $LaAlO_3$, which means that the angle of misorientation $\theta$ between the film and the substrate is 0°. The $\rho$–$T$ curves of both sides of YBCO films measured by the four probe method are shown in Fig. 4. Both $\rho$–$T$ curves have almost the same features and $T_c$(zero) of side I and II are 90 K and 86 K, respectively. From the results of $\theta$–$2\theta$ scan, pole figure measurement, SEM image, and $T_c$ measurement on both sides of the film of the $LaAlO_3$ (100) substrate, the homogeneity was very good.

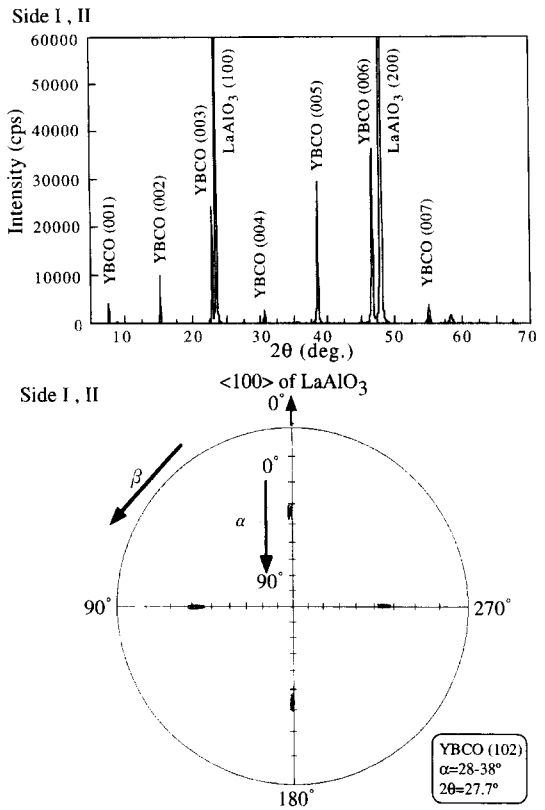


Fig. 3. The $\theta$–$2\theta$ scan and the pole figure of (102) reflection of the both sided YBCO films (side I and II).

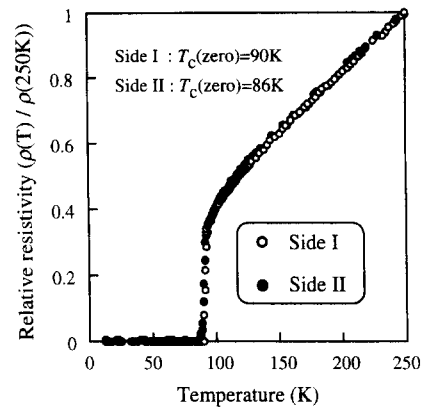


Fig. 4. The $\rho$–$T$ curves normalized by the resistivity at 250 K for both sided YBCO films measured by four probe method.

### 3.2. Homogeneity of the film along the source gas flow direction

It was expected that homogeneity of the films along the source gas flow direction was not good due to the variation of deposition temperature. For the first step, we deposited YBCO films without pulling up the sample holder. We divided the grown YBCO films into four parts along the flow direction ((a)–(d)) in Fig. 2, where (a) was the topmost part above the stream of the source gas flow. $T$(a), the atmospheric temperature, was 680°C. Each part of the film was characterized by XRD, pole figure, SEM and SQUID measurements. XRD patterns of all parts of the films showed $c$-axis orientation and pole figure patterns of them showed four-fold symmetry. SEM images show that microstructure of the topmost part (a) is the coalescence of small size grains, whereas the film surface of the bottom part of the films (d) indicates melting. Both (b) and (c) have smooth surfaces with some precipitations. Fig. 5 shows magnetic susceptibilities of each film measured by SQUID magnetometer. The curves of Fig. 5(b) and (c) sharply drop at 90 K and suggest the superconductive quality of the films is satisfactory. But susceptibility of the part (a) shows incomplete drop even at low temperatures, that means the superconducting ratio of this part is

very small. Fig. 5(d) is a gradually decreasing curve toward low temperatures, which means the film is a mixture of superconductors having different critical temperatures.

From these results, the homogeneity of the films seems to be poor, which may be due to the different

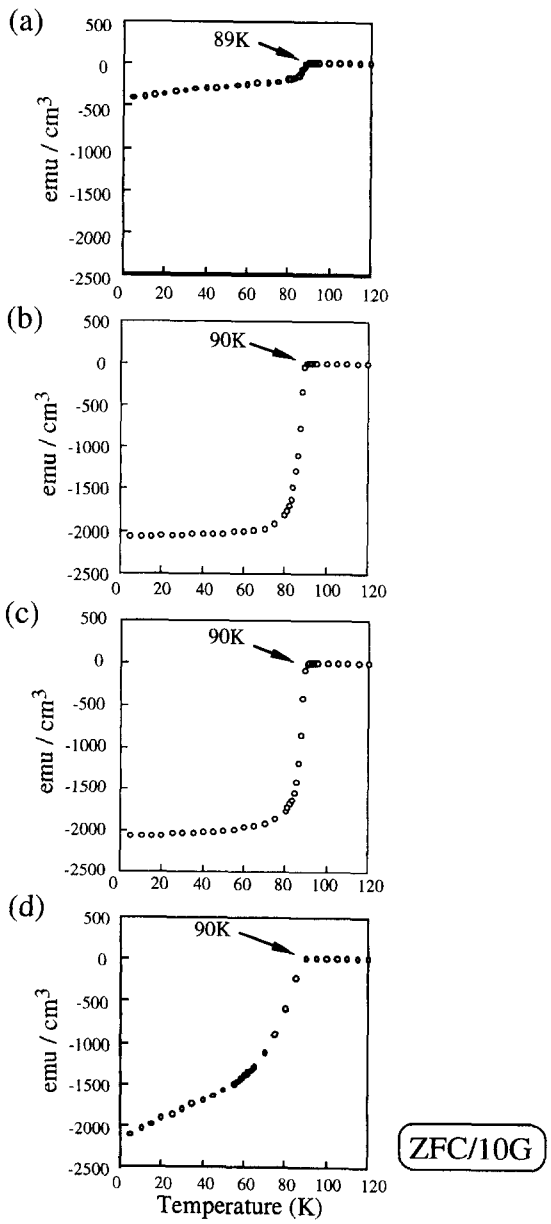


Fig. 5. Magnetic susceptibilities of each YBCO film without the pulling up procedure measured by SQUID magnetometer. (a)–(d) stand for the points shown in Fig. 2.

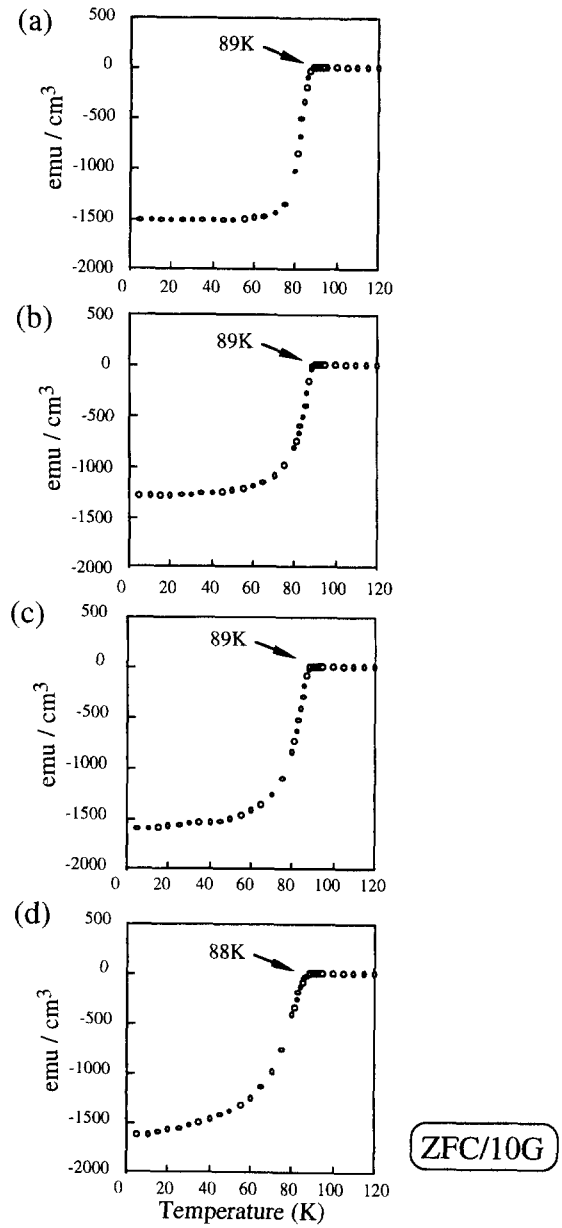


Fig. 6. Magnetic susceptibilities of each YBCO film with the pulling up procedure measured by SQUID magnetometer. (a)–(d) stand for the points shown in Fig. 2.

deposition conditions. The most suitable deposition area is only between the points (b) and (c) which are about 10 mm in length. Then we tried to pull up the sample substrate during the deposition term to improve homogeneity. The pulling up procedure was as

follows: we set the upper half part of the substrate, which was 20 mm in length, at the most suitable deposition area and deposited YBCO films in 1 h, then we pulled up the substrate at 90 mm/h until the lower half part came to the most suitable deposition area and deposited films again. All parts of the YBCO films grown with the pulling up procedure showed identical properties to the best part of the stationarily deposited films which were the highly *c*-axis oriented and biaxially aligned in the *ab*-plane. The surface morphologies by SEM observation were also identical. Fig. 6 shows the magnetic susceptibility curves of the film grown with the pulling up procedure. Compared with the results of stationarily deposited films, the curve of the topmost part (a) of the film sharply dropped at around 90 K. Fig. 7 shows the comparison for local superconducting volume of the films with and without the pulling up procedure. The result indicates that the homogeneity

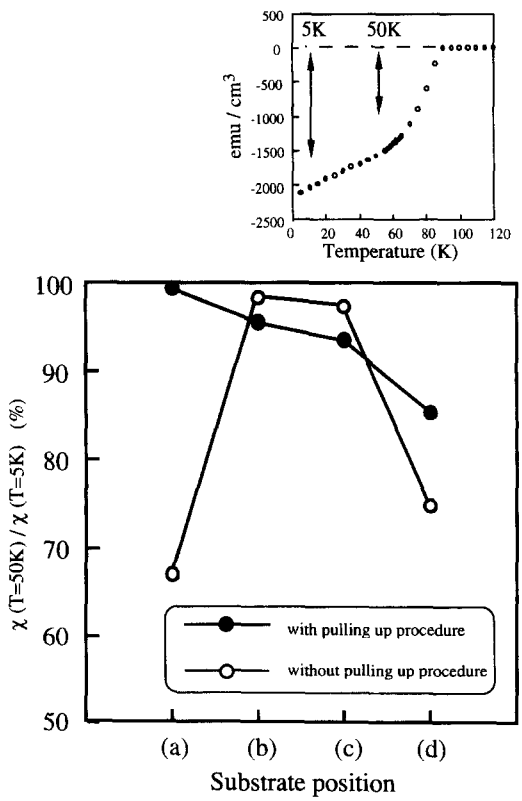


Fig. 7. Comparison for local superconducting volume of the films with and without the pulling up procedure (normalized at 5 K). (a)–(d) stand for the points shown in Fig. 2.

Fig. 8. A photograph of YBCO-coated fiber on the single crystalline $SrTiO_3$ fiber.

of YBCO films along the source gas flow direction was remarkably improved. The reason why is that all parts of the film pass through the optimal deposition area by the pulling up procedure.

### 3.3. Deposition of YBCO on the fine single crystalline $SrTiO_3$ fiber

Deposition onto the $SrTiO_3$ fiber having a (100) facet was performed in the similar way onto the double-sided polished substrates. The films grown on the fiber showed the biaxially aligned orientation on the facet. From the $\rho$–$T$ curve measured by the four probe method, $T_c$(onset) = 92 K and $T_c$(zero) = 72 K were obtained for the film on the $SrTiO_3$ fiber. After deposited YBCO films on the fiber by MOCVD, we thickened the YBCO layer by the liquid phase epitaxy (LPE) method [11]. Fig. 8 shows a photograph of YBCO-coated fiber on the $SrTiO_3$ fiber. Enlarged SEM image of the YBCO film which was thickened by LPE was shown in Fig. 9. Although growth of the YBCO film was confirmed on the whole surface of facet, several microcracks were observed on the film.

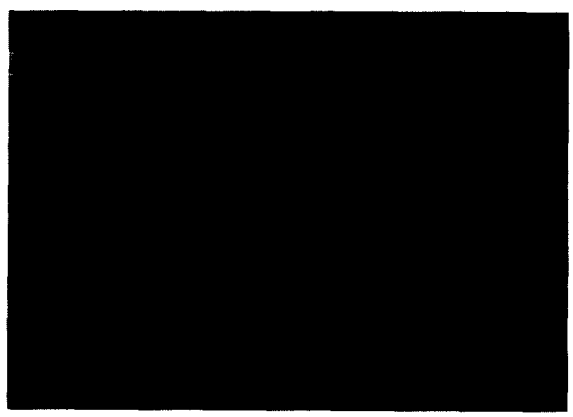

Fig. 9. SEM image of LPE-coated YBCO on the single crystalline $SrTiO_3$ fiber.

Therefore, in order to obtain transport properties, eliminating the crack is necessary.

## 4. Conclusions

We developed a hot-wall type MOCVD apparatus for the deposition of YBCO onto both sides of the substrates and onto the arbitrary shaped substrates. By improving the reactor shape and gas flow of the source materials, we succeeded in fabricating YBCO films both on the double-sided polished $LaAlO_3$ (100) substrates and on the fine single crystalline $SrTiO_3$ fibers. The $T_c$(zero) values of each side were 90 and 86 K, respectively, for the double-sided YBCO films on the $LaAlO_3$ substrates. Homogeneity of the films along the source gas flow direction was remarkably improved by the pulling up procedure. Superconducting properties were almost uniform within the YBCO films of 20 mm length. The YBCO films on the facet of single crystalline $SrTiO_3$ fiber were biaxially aligned, and enabled us to prepare YBCO thick films by LPE.

## Acknowledgements

This work was supported by the New Energy and Industrial Technology Development Organization (NEDO) for R&D of Industrial Science and Technology Frontier Program.

## References

[1] T. Yoshitake, H. Tsuge, T. Inui, S. Suzuki, Jpn. J. Appl. Phys. 33 (1994) L1156.
[2] P. Bodin, J.L. Skov, A. Kuhle, M. Hagensen, T. Clausen, I. Rasmussen, S. Hjorth, J.B. Hansen, Superconduct. Sci. Technol. 7 (1994) 717.
[3] D.W. Face, C. Wilker, Z.-Y. Shen, P. Pang, R.J. Small, IEEE Trans. Appl. Superconduct. 5 (1995) 1581.
[4] Z. Lu, J.K. Truman, M.E. Johansson, D. Zhang, C.F. Shih, G.C. Liang, Appl. Phys. Lett. 67 (5) (1995) 712.
[5] K. Onabe, O. Kohno, S. Nagaya, T. Shimonosono, Y. Iijima, N. Sadakata, T. Saito, Mater. Trans. JIM 37 (4) (1996) 893.
[6] D.P. Norton, A. Goyal, J.D. Budai, D.K. Christen, D.M. Kroeger, E.D. Specht, Q. He, B. Saffian, M. Paranthaman, C.E. Klabunde, D.F. Lee, B.C. Sales, F.A. List, Science 274 (1996) 755.
[7] J. Kawashima, T. Kitamura, S. Taniguchi, Y. Niiori, Y. Shiohara, I. Hirabayashi, S. Tanaka, Advances in Superconductivity VIII, Springer, Tokyo, 1995, p. 767.
[8] M. Matsubara, K. Higashiyama, I. Hirabayashi, Advances in Superconductivity V, Springer, Tokyo, 1992, p. 837.
[9] Y. Ito, Y. Yoshida, Y. Mizushima, I. Hirabayashi, H. Nagai, Y. Takai, Jpn. J. Appl. Phys. 35 (1996) L825.
[10] H. Nagai, Y. Yoshida, Y. Ito, S. Taniguchi, I. Hirabayashi, N. Matsunami, Y. Takai, Superconduct. Sci. Technol. 10 (1997) 213.
[11] Y. Yamada, Y. Niiori, Y. Yoshida, I. Hirabayashi, S. Tanaka, J. Cryst. Growth 167 (1996) 566.